# Design of Phased Array Architectures for Full-Duplex Joint Communications and Sensing

Mikko Heino, Carlos Baquero Barneto, Taneli Riihonen, and Mikko Valkama

Electrical Engineering, Faculty of Information Technology and Communication Sciences, Tampere University, Finland

mikko.heino@tuni.fi

*Abstract*—The short wavelength of millimeter-waves in fifth-generation (5G) mobile communications enables the implementation of multi-element antenna arrays in relatively small space, e.g., in user devices and small base stations. Joint communication and sensing (JCAS) is a scheme which utilizes the beamsteering capabilities of the multi-element antenna arrays for simultaneously maintaining a communication link and sensing the surroundings with a radar beam and receiving it with the same device. The simultaneous transmission and reception requires a beam weighting algorithm which cancels the self-interference while at the same time maintaining the integrity of both beams. In this paper, the performance of different linear patch antenna array architectures is studied in terms of self-interference cancellation performance and obtained maximum gain in the beamsteering range. A mirror-beam problem in the self-interference cancellation algorithm for parallel arrays is studied and novel coupling randomization is introduced for the arrays to prevent the forming of the mirror beams.

*Index Terms*—Joint communications and sensing, antenna coupling, in-band full-duplex, phased array antennas.

## I. INTRODUCTION

In the fifth-generation (5G) and beyond mobile communication systems, millimeter-wave (mm-wave) frequency bands are utilized to obtain highly increased communication capacity. The wide bandwidths available at mm-waves enable also accurate radio-based sensing and localization schemes, which have been of great interest in civilian and professional applications. Thus, there is a common interest for communication and sensing at the same frequency bands which leads to radio spectrum congestion.

The research into radio-frequency (RF) convergence has become an important research area where the same frequency bands are used for both communication and sensing operations [1]. Especially in joint communication and sensing (JCAS) systems, both functionalities are performed by sharing the same transmit signals and the same hardware platforms [2]. Potential applications for the JCAS systems include autonomous vehicle networks [3], unmanned aerial vehicle (UAV) control systems, and mobile networks with sensing capabilities in the base stations and user devices [4], [5]. For example, a mm-wave user device could sense its surroundings while simultaneously maintaining a communication link to the base station, or vice versa, the small base station could monitor its environment.

However, the major problem in JCAS systems is the coupling of the strong self-interference (SI) from the transmitting



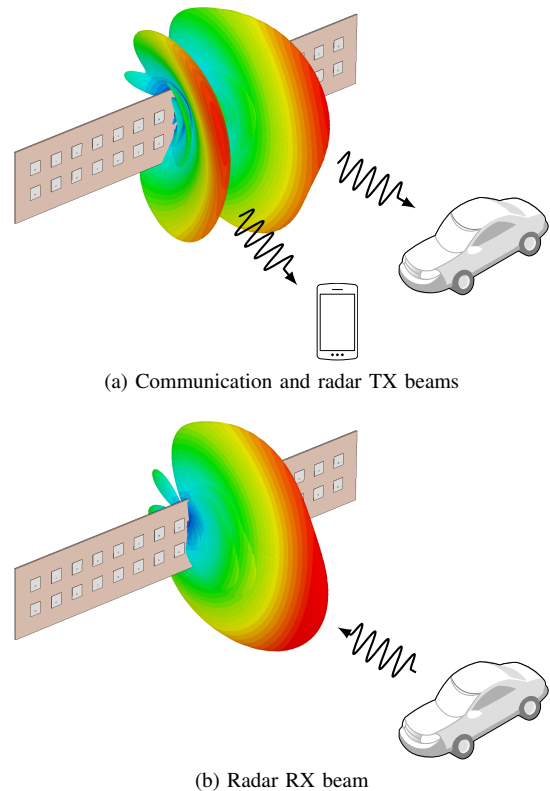(a) Communication and radar TX beams



(b) Radar RX beam

Fig. 1. The simultaneous (a) transmitter and (b) receiver beams in joint communication and sensing (JCAS) operation.

(TX) antenna to the receiving (RX) antenna. Thus, the enabler for JCAS is in-band full-duplex (IBFD) operation, that is also known as simultaneous transmit-and-receive (STAR) operation. This is because typical communication frames are so long that pulse radar operation is impossible. In previous literature, IBFD and SI cancellation have been widely researched for communication purposes [6]. However, JCAS is different in the sense that the goal is to cancel only the direct leakage between the TX and RX antenna arrays, while preserving the useful reflections of the radar beam from the environment which are used for the sensing. Figure 1 illustrates the concept of separate beams for parallel 16-element RX and TX antenna arrays for JCAS operation.

The initial research in JCAS has focused on single-beam approaches for the TX and RX antenna antenna array limiting the sensing direction to the same as for the communication link. Recent studies have raised the idea of using simultaneous

separate beams for communication and sensing purposes in the transmitter, while only receiving from the direction of the transmitted radar beam [7]. In this paper, a novel beamforming approach is used which enables separate radar and communication beams in the transmitter, while at the same time receiving the sensing information from the radar beam direction and cancelling the directly coupled SI [8]. However, the performance of the SI cancelling algorithm depends on the coupling and symmetry of the transmit and receive arrays. Array SI cancellation has been previously studied in 2D arrays by either feeding different TX elements in opposite phase [9] or utilizing filtered copies of the transmit signal and subtracting them from the receive signal [10]. However, the research so far does not consider design of array architectures for JCAS operation utilizing only the beamforming weights without limiting the beamsteering range.

This paper resolves the design of good antenna array architectures for operation with a SI-cancelling JCAS algorithm. Emphasis is on uniform linear arrays (ULAs) with 16 patch antenna elements in the azimuth plane for both receiving and transmitting arrays (cf. Fig. 2). The effect of symmetry in the coupling between the TX and RX antenna arrays and the most efficient arrangement of the antenna arrays is studied and conclusions are made about the best antenna array properties for JCAS operation. A mirror beam problem is identified in the SI cancellation algorithm and a novel array with randomized coupling is introduced to solve the issue.

## II. JCAS Beamforming

The JCAS array utilizes a communication beam and a radar beam to sense its surroundings in the transmitter. Let $\mathbf{x}(t) = \mathbf{w}_{\mathrm{TX}}s(t)$ denote the radiated waveform transmitted from the JCAS system, where $s(t)$ refers to the TX joint communication–radar waveform. This radiated waveform propagates over-the-air and interacts with one or multiple targets, producing reflections that will be collected by the RX system [7] for sensing purposes with the radar beam.

While the array responses are obtained from simulated electromagnetic fields, for calculating the array beam weights for the transmitter and the receiver, an ideal model for an linear uniform antenna array response is used as described by

$$\mathbf{a}_{\mathrm{TX}}(\theta) = \mathbf{a}_{\mathrm{RX}}(\theta) = \left[1, e^{jkd\sin(\theta)}, \ldots, e^{jkd(N-1)\sin(\theta)}\right]^T,$$
(1)

where $d$ and $k$ denote the antenna spacing and the wavenumber, respectively. The TX weights are obtained separately for the communication beam $\mathbf{w}_{\mathrm{TX,C}}$ and radar beam $\mathbf{w}_{\mathrm{TX,R}}$ as

$$\mathbf{w}_{\mathrm{TX,C}} = \frac{\mathbf{a}_{\mathrm{TX}}^*(\theta_{\mathrm{C}})}{\|\mathbf{a}_{\mathrm{TX}}(\theta_{\mathrm{C}})\|} \text{ and } \mathbf{w}_{\mathrm{TX,R}} = \frac{\mathbf{a}_{\mathrm{TX}}^*(\theta_{\mathrm{R}})}{\|\mathbf{a}_{\mathrm{TX}}(\theta_{\mathrm{R}})\|},$$
(2)

where $\theta_{\mathrm{C}}$ and $\theta_{\mathrm{R}}$ are the communication and radar beam directions, respectively. The operators $(\cdot)^*$ and $\|\cdot\|$ refer to the conjugate complex operation and the Euclidean norm, respectively. In the particular case of ideal ULAs per (1), the optimal beamforming weights are calculated such that

$$w_n(\theta) = \frac{1}{\sqrt{N}}e^{-jkdn\sin\theta},$$
(3)



(a) Parallel 16-element RX/TX arrays

(b) Parallel 16-element RX/TX arrays with coupling randomized
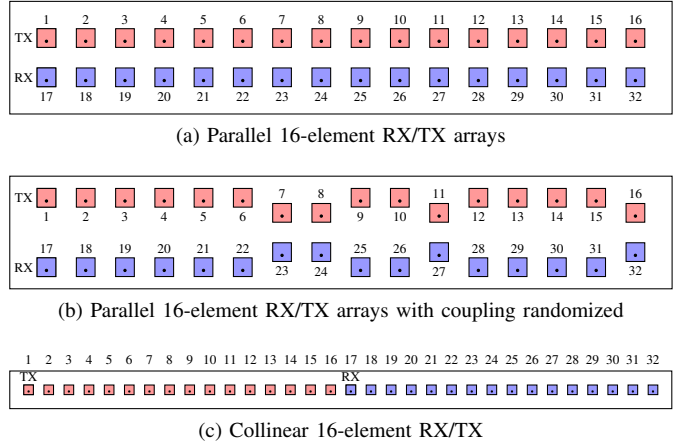
(c) Collinear 16-element RX/TX

Fig. 2. Studied linear antenna array architectures.

where $n \in [0, N-1]$ refers to the antenna element index. Then the weights are combined coherently as

$$\mathbf{w}_{\mathrm{TX}} = \sqrt{\rho}\mathbf{w}_{\mathrm{TX,C}} + \sqrt{1-\rho}\mathbf{w}_{\mathrm{TX,R}},$$
(4)

where $0 \leq \rho \leq 1$ controls the power allocation between both radar and communication beam.

The RX array weights $\mathbf{w}_{\mathrm{RX}}$ are selected such that they are projected to the null-space of the SI expressed by

$$\mathbf{w}_{\mathrm{RX}}^T\mathbf{H}_{\mathrm{SI}}(f)\mathbf{w}_{\mathrm{TX}} = 0,$$
(5)

where $\mathbf{H}_{\mathrm{SI}}(f)$ is a narrowband self-interference matrix, i.e., the coupling between the RX and TX antenna array elements in free space at point frequency $f$. However, since usually self-interference cancellation at single frequency is not enough for wideband cancellation, the method can be extended to project to the null space at multiple point frequencies simultaneously:

$$\mathbf{w}_{\mathrm{RX}}^T\underbrace{\left[\mathbf{H}_{\mathrm{SI}}(\phi_1)\mathbf{w}_{\mathrm{TX}}, \ldots, \mathbf{H}_{\mathrm{SI}}(\phi_{\mathcal{N}})\mathbf{w}_{\mathrm{TX}}\right]}_{=\mathbf{X}} = \mathbf{0},$$
(6)

where $\mathcal{N}$ denotes the number of frequency nulls at frequencies $\phi_n$, $n = 1, 2, \ldots, \mathcal{N}$. The RX weights are calculated as a combination of a null-space projection (NSP) matrix, where $\mathbf{X}^+$ denotes the pseudoinverse of $\mathbf{X}$, and a matched filter as

$$\mathbf{w}_{\mathrm{RX}} = \frac{((\mathbf{I} - \mathbf{X}^+\mathbf{X})\mathbf{a}_{\mathrm{RX}}(\theta_{\mathrm{R}}))^*}{\|(\mathbf{I} - \mathbf{X}^+\mathbf{X})\mathbf{a}_{\mathrm{RX}}(\theta_{\mathrm{R}})\|}.$$
(7)

This yields maximum gain with a single beam in the radar direction $\theta_{\mathrm{R}}$ under the constraint of simultaneously cancelling self-interference at the $\mathcal{N}$ point frequencies (cf. Fig. 3). The beamforming scheme has been presented in detail in [8].

The average amount of cancellation across the whole operational band can be calculated by

$$\mathrm{C}_{\mathrm{SI}} = \frac{1}{M}\sum_{m=1}^{M}\left|\mathbf{w}_{\mathrm{RX}}^T\mathbf{H}_{\mathrm{SI}}(f_m)\mathbf{w}_{\mathrm{TX}}\right|^2,$$
(8)

where $f_m \in [27.75, 28.25]$ GHz, $m = 1, 2, \ldots, M$, for all the $M$ point frequencies for which the array architectures are simulated — see, e.g., Fig. 4 for the architectures of Fig. 2.

## III. JCAS Array Architectures

For both the receiving and transmitting sides, $1{\times}16$ antenna arrays operating at the center frequency of 28 GHz with system bandwidth of 500 MHz are investigated, considering $M = 501$ discretized and equidistant frequencies. The arrays consist of patch antennas implemented on a 0.305 mm thick Rogers 4003C substrate with copper cladding thickness of 35 $\mu$m.

The simulated array architectures are shown in Fig. 2. In particular, we consider three array configurations as follows:

- parallel 16-element arrays with uniform 5.35 mm spacing between TX and RX antenna arrays — Fig. 2(a),
- parallel 16-element arrays with randomized 9.46 mm or 5.35 mm TX–RX spacing — Fig. 2(b),
- collinear 16-element TX and RX antenna arrays which form a 32-element uniform linear array — Fig. 2(c).

The individual patch elements with the size of $2.55{\times}2.55$ mm$^2$ are fed with coaxial cables from the other side of the PCB. The total size of parallel patch arrays in Figs. 2(a) and 2(b) is $91.6{\times}15.4$ mm$^2$, whereas the size of the collinear array in Fig. 2(c) is $175.9{\times}10$ mm$^2$. In all cases the inter-element distance is $d = \lambda_0/2 = 5.35$ mm at 28 GHz, where $\lambda_0$ is the free-space wavelength.

For each architecture, TX weights are the same corresponding to radar and communication beam angles. The power is allocated equally to radar and communication beams, thus $\rho = 0.5$. The RX weights are chosen differently for each array depending on the coupling matrix between TX and RX elements. Figure 3 shows the typical performance of optimizing the RX weighs with the self-interference cancellation algorithm by increasing the number of frequency nulls.

### A. Cancellation Performance with the Parallel Arrays

By utilizing two parallel 16-element patch antenna arrays for the RX and TX in Fig. 2(a), the cancellation performance is seen in Fig. 3 when changing the number of cancellation nulls in (6) with communication beam direction $\theta_C = -20°$ and radar direction $\theta_R = 10°$. The frequencies of the nulls are chosen symmetrically around the center frequency so that the average coupling level of the whole band is minimized. Increasing the number of nulls $\mathcal{N}$ decreases the obtainable peak gain for the radar beam at maximum 0.6 dB with $\mathcal{N} = 3$ for some radar angles, but this improves greatly the obtained wideband SI cancellation. It is seen that by nulling $\mathcal{N} = 3$ frequencies, it is possible to reduce the SI to levels below -100 dB for the whole band. However, this requires a very accurate SI-channel estimate between the TX and RX array.

Fig. 4 shows the obtained average cancellation for the analyzed array configurations as a function of the radar beam angle when the communication beam is fixed at $\theta_C = -20°$.

### B. Problematic Mirror Beams

For beamsteering combinations when $\theta_C = -\theta_R$ or $\theta_R = 0°$, mirror beams are generated in the RX array pattern for the parallel RX/TX array. This effect is illustrated in Fig. 8a where the RX pattern is plotted in the case of $\theta_C = -\theta_R =$
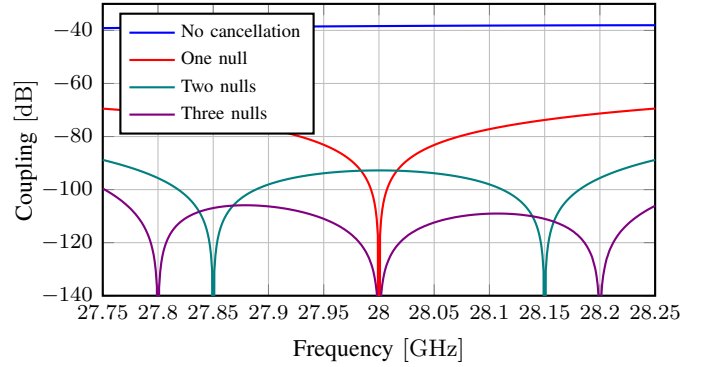


Fig. 3. SI-cancellation in the operating band when increasing the number of cancellation nulls $\mathcal{N}$ for the parallel RX/TX arrays.
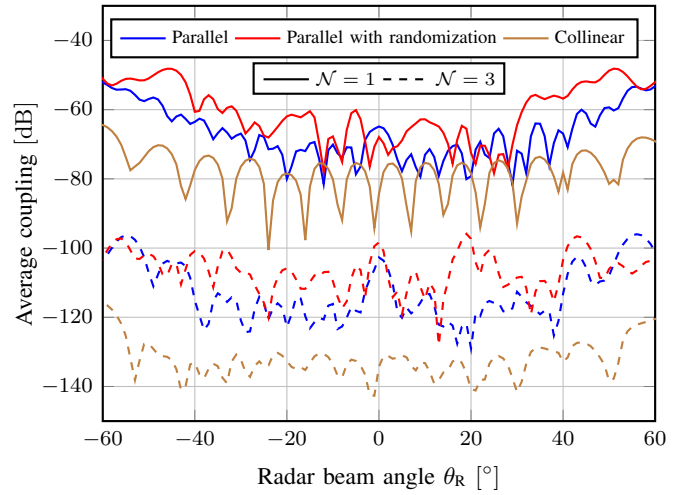


Fig. 4. Average cancellation obtained for the frequency band 27.75 GHz to 28.25 GHz with $\mathcal{N} = 1$ and $\mathcal{N} = 3$ frequency nulls.

$-30°$. This is caused by the lack of phase variance in the SI-vector received by the RX array. In a typical case when $\theta_C \neq -\theta_R \neq 0°$, the TX weights are a superposition of two different complex phasor beam coefficients with different linear phase shift between the elements. This superposition causes a high variance in the phase of the received SI of each RX antenna element $\mathbf{H}_{SI}(f)\mathbf{w}_{TX}$. However, when $\theta_C = -\theta_R$ or $\theta_R = 0°$, the TX weights reduce to real values or to a sum of constant value with single phasor with linear phase shift. Figures 5(a) and 6(a) show the coupled SI to each RX element when $\theta_R = 10°$ or $\theta_R = 0°$, while $\theta_C = -20°$. It is seen that the phase range of the coupled SI is limited when $\theta_R = 0°$.

The above is explained by the operation of the NSP algorithm. When the SI has strong variance in phase as in Fig. 5(a), the NSP algorithm is able to minimize the sum of the SI by only tuning the amplitudes of RX weights to balance out the received SI components so that they cancel each other out as seen in Fig. 5(b). This causes minimal changes to the phases of the RX weights which would change the direction of the beam. However, for the case in Fig. 6(a), the algorithm needs also to

tune the phases of the RX weights to be able to bring the sum $\mathbf{w}_{RX}^T \mathbf{H}_{SI}(f)\mathbf{w}_{TX}$ down to zero which causes the mirror beam. The mirror beam problem also happens when $\theta_C = -\theta_R$ as then the resulting TX weights are scalar causing limited phase variance also in the coupled SI $\mathbf{H}_{SI}(f)\mathbf{w}_{TX}$.

### C. Coupling Randomization for Avoiding Mirror Beams

To solve the problem with the mirror beams caused in the symmetric parallel array configuration, an alternative array configuration is proposed. In this architecture, the distance between some RX/TX antenna element pairs has been increased to 9.46 mm as seen in Fig. 2(b). This adds a $180°$ phase delay to some elements of the SI-vector received by the RX array. This creates a wider variance of phases in the SI-vector, and enables the NSP algorithm to cancel the SI without effect to the radar beam by mainly balancing the amplitudes of the RX weights. The coupled SI-vector and the RX weights are seen in Figs. 6(c) and 6(d) for the randomized array. As it is seen in the azimuth plane in Figs. 8a and 8b, the mirror beams disappear after applying the array randomization. In the elevation plane, the effect of the offset of the few elements is minimal.

The maximum gains when sweeping the radar beam across the beam angular range are seen in Fig. 9. It is seen that the randomization improves the RX radar beam gain at $\theta_R = 0°$ and at the mirror angle $\theta_R = 20°$ up to 2 dB. However, the obtainable average SI-cancellation level by the algorithm decreases 5 to 10 dB as seen in Fig. 4. Still, when increasing the number of nulls in the cancellation to three, the SI can be decreased down to levels below -100 dB for both cases.

### D. Cancellation Performance with the Collinear Arrays

The third option to arrange the arrays is to have the both RX and TX arrays on the same line side-by-side as seen in Fig. 2(c). This doubles the overall width of the array. However, the SI-cancellation performance is better than for the both parallel arrays, as the overall coupled SI-power is smaller as the RX and TX arrays are further away from each other. The main coupling is caused by the element 16 of TX array and the element 17 of the RX array.

The collinear arrays inherently avoid the mirror beam problem. As is seen from Fig. 7(a), the coupled SI to each RX element is a lot smaller than for the parallel arrays, and the phase of the SI components varies between two phase values with difference of $180°$. This is caused by the fact that the element 16 of the TX array is the main contributor to the SI for the RX array, and each RX array element is separated $\lambda_0/2$ from each other, thus resulting in $\pm180°$ variance in the received SI of each element. Figs. 8b and 8a show the beams where $\theta_R = 0°$ and $\theta_R = -\theta_C$ indicating the absence of the mirror beams for the collinear arrays.

### E. Guidelines for JCAS Array Design

The mirror beam problem of the parallel arrays is caused by strong correlation of the RX element self-interference with the corresponding TX element weight. The mirror beams were visible for beam angles $\theta_R = 0°$ and $\theta_R = -\theta_C$ and they can be
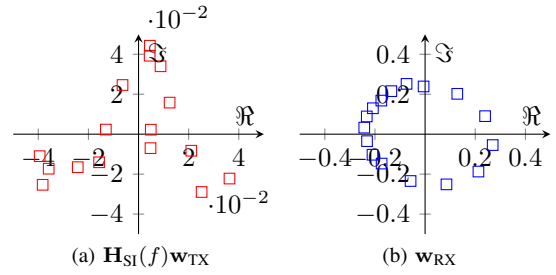


Fig. 5. SI received by each RX element in parallel RX/TX arrays and the generated RX weights for radar direction $\theta_R = 10°$ at 28 GHz. ($\theta_C = -20°$)



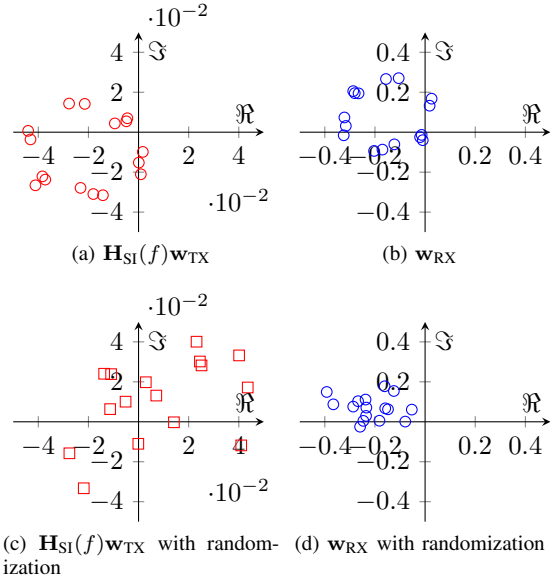(c) $\mathbf{H}_{SI}(f)\mathbf{w}_{TX}$ with randomization (d) $\mathbf{w}_{RX}$ with randomization

Fig. 6. SI received by each RX element in parallel RX/TX arrays and the generated RX weights with/without randomization for radar direction $\theta_R = 0°$ at 28 GHz. ($\theta_C = -20°$)

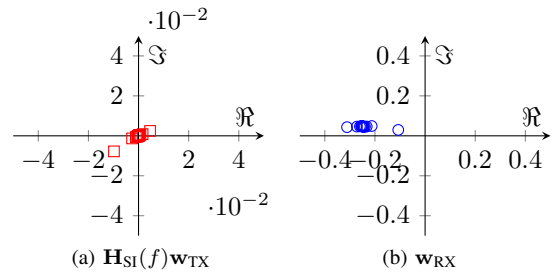

Fig. 7. SI received by each RX element in collinear RX/TX arrays and the generated RX weights for radar direction $\theta_R = 0°$ at 28 GHz. ($\theta_C = -20°$)

reduced with randomization in the individual RX–TX element distances that reduces the phase correlation in the SI-vector.

In summary, the following guidelines are obtained for efficient antenna array design for JCAS:

- Collinear patch TX and RX antenna arrays are good for JCAS due to the phase distribution of the coupled SI. The $\lambda_0/2$ distance between each RX element causes a $180°$ phase shift for SI-vector elements which benefits the SI cancellation algorithm and removes the mirror beams.
- Usage of non-uniform TX–RX element pair distances in parallel patch antenna arrays enables avoiding mirror beams if a more compact antenna array is needed.
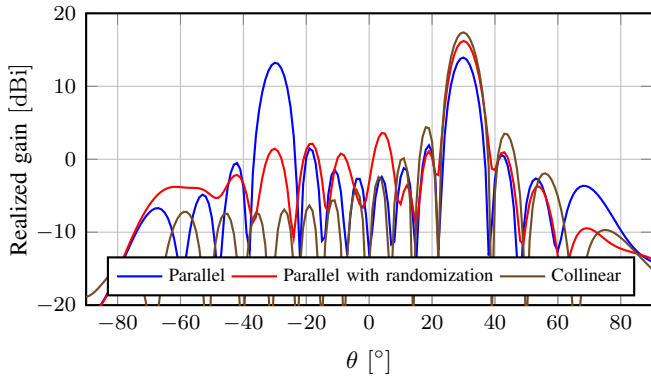
(a) $\theta_R = 30°$ and $\theta_C = -30°$
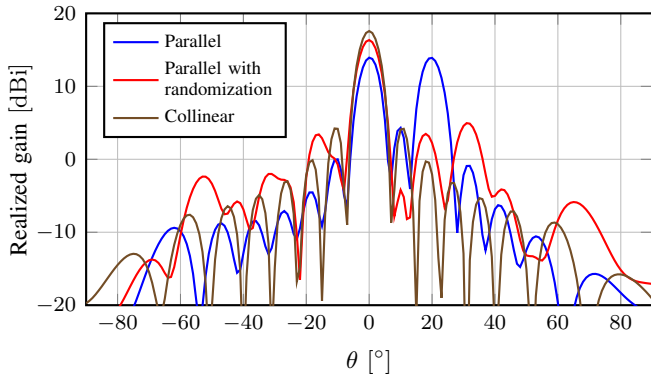


(b) $\theta_R = 0°$ and $\theta_C = -20°$

Fig. 8. RX antenna array radar beam with radar direction $\theta_R$ and communication direction $\theta_C$ with SI cancellation using $\mathcal{N} = 1$ frequency null at 28 GHz.

- The SI cancellation algorithm is able to cancel the self-interference below $-100$ dB if three frequency nulls are used for each type of antenna array.

## IV. CONCLUSION

This paper studied the performance of different linear patch array architectures in a JCAS application. The arrays were studied under a novel self-interference cancellation algorithm which is required for true in-band full-duplex JCAS operation in the same frequency band. The study shows a mirror beam problem associated with parallel arrays which is caused by strong correlation of the RX element self-interference with the corresponding TX element weight. A novel parallel array configuration was introduced with randomization in the individual RX–TX element distances, to reduce the phase correlation in the SI-vector, which removed the mirror beams. We are currently generalizing the multibeam concept to joint MIMO communications with MIMO radar [11], where the same mirror beam challenge needs to be addressed too.
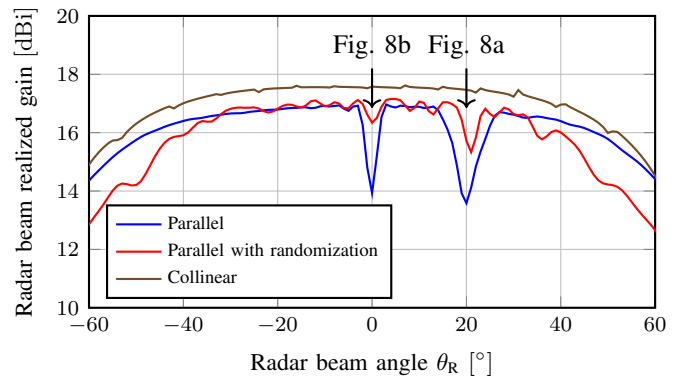


Fig. 9. Sweeping the RX radar beam with TX communication beam to direction $\theta_C = -20°$ with SI cancellation using $\mathcal{N} = 1$ frequency null at 28 GHz.

## REFERENCES

[1] B. Paul, A. R. Chiriyath, and D. W. Bliss, "Survey of RF communications and sensing convergence research," *IEEE Access*, vol. 5, pp. 252–270, Jan. 2017.

[2] F. Liu, C. Masouros, A. P. Petropulu, H. Griffiths, and L. Hanzo, "Joint radar and communication design: Applications, state-of-the-art, and the road ahead," *IEEE Transactions on Communications*, vol. 68, no. 6, pp. 3834–3862, Jun. 2020.

[3] P. Kumari, J. Choi, N. González-Prelcic, and R. W. Heath, Jr., "IEEE 802.11ad-based radar: An approach to joint vehicular communication–radar system," *IEEE Transactions on Vehicular Technology*, vol. 67, no. 4, pp. 3012–3027, Apr. 2018.

[4] M. L. Rahman, J. A. Zhang, X. Huang, Y. J. Guo, and R. W. Heath, Jr., "Framework for a perceptive mobile network using joint communication and radar sensing," *IEEE Transactions on Aerospace and Electronic Systems*, vol. 56, no. 3, pp. 1926–1941, Jun. 2020.

[5] F. Guidi, A. Guerra, and D. Dardari, "Personal mobile radars with millimeter-wave massive arrays for indoor mapping," *IEEE Transactions on Mobile Computing*, vol. 15, no. 6, pp. 1471–1484, Jun. 2016.

[6] K. E. Kolodziej, B. T. Perry, and J. S. Herd, "In-band full-duplex technology: Techniques and systems survey," *IEEE Transactions on Microwave Theory and Techniques*, vol. 67, no. 7, pp. 3025–3041, Jun. 2019.

[7] C. Baquero Barneto, S. D. Liyanaarachchi, T. Riihonen, L. Anttila, and M. Valkama, "Multibeam design for joint communication and sensing in 5G new radio networks," in *Proc. IEEE International Conference on Communications*, Jun. 2020.

[8] C. Baquero Barneto, S. D. Liyanaarachchi, T. Riihonen, M. Heino, L. Anttila, and M. Valkama, "Beamforming and waveform optimization for OFDM-based joint communications and sensing at mm-waves," in *Proc. 54th Asilomar Conference on Signals, Systems, and Computers*, Nov. 2020.

[9] T. Snow, C. Fulton, and W. J. Chappell, "Transmit–receive duplexing using digital beamforming system to cancel self-interference," *IEEE Transactions on Microwave Theory and Techniques*, vol. 59, no. 12, pp. 3494–3503, Dec. 2011.

[10] I. T. Cummings, J. P. Doane, T. J. Schulz, and T. C. Havens, "Aperture-level simultaneous transmit and receive with digital phased arrays," *IEEE Transactions on Signal Processing*, vol. 68, pp. 1243–1258, Jan. 2020.

[11] S. D. Liyanaarachchi, C. Baquero Barneto, T. Riihonen, M. Heino, and M. Valkama, "Joint multi-user communication and MIMO radar through full-duplex hybrid beamforming," in *Proc. 1st IEEE International Online Symposium on Joint Communications and Sensing*, Feb. 2021.